PLOS ONE

RESEARCH ARTICLE

Molecular dynamics study on characteristics of reflection and condensation molecules at vapor–liquid equilibrium state

Hirofumi Tabe*, Kazumichi Kobayashi, Hiroyuki Fujii, Masao Watanabe

Division of Mechanical and Space Engineering, Hokkaido University, Sapporo, Hokkaido, Japan

* azx@eis.hokudai.ac.jp

Citation: Tabe H, Kobayashi K, Fujii H, Watanabe M (2021) Molecular dynamics study on characteristics of reflection and condensation molecules at vapor–liquid equilibrium state. PLoS ONE 16(3): e0248660. https://doi.org/10.1371/journal.pone.0248660

Editor: Bing-Yang Cao, Tsinghua University, CHINA

Received: December 23, 2020

Accepted: March 3, 2021

Published: March 16, 2021

Data Availability Statement: All relevant data are within the paper and its Supporting information files.

Funding: This work was supported by JSPS KAKENHI Grant Number JP20K04277 to K.K. (https://www.jsps.go.jp/english/index.html) and f3 Engineering Education and Research Center, Faculty of Engineering, Hokkaido University to K.K. The funders had no role in study design, data collection and analysis, decision to publish, or preparation of the manuscript.

Abstract

The kinetic boundary condition (KBC) represents the evaporation or condensation of molecules at the vapor–liquid interface for molecular gas dynamics (MGD). When constructing the KBC, it is necessary to classify molecular motions into evaporation, condensation, and reflection in molecular-scale simulation methods. Recently, a method that involves setting the vapor boundary and liquid boundary has been used for classifying molecules. The position of the vapor boundary is related to the position where the KBC is applied in MGD analyses, whereas that of the liquid boundary has not been uniquely determined. Therefore, in this study, we conducted molecular dynamics simulations to discuss the position of the liquid boundary for the construction of KBCs. We obtained some variables that characterize molecular motions such as the positions that the molecules reached and the time they stayed in the vicinity of the interface. Based on the characteristics of the molecules found from these variables, we investigated the valid position of the liquid boundary. We also conducted an investigation on the relationship between the condensation coefficient and the molecular incident velocity from the vapor phase to the liquid phase. The dependence of the condensation coefficient on the incident velocity of molecules was confirmed, and the value of the condensation coefficient becomes small in the low-incident-velocity range. Furthermore, we found that the condensation coefficient in the non-equilibrium state shows almost the same value as that in the equilibrium state, although the corresponding velocity distribution functions of the incident velocity significantly differ from each other.

1 Introduction

Gas or vapor flows in the non-equilibrium region in the vicinity of the vapor–liquid interface can be investigated based on molecular gas dynamics (MGD) [1–3], which is described using the velocity distribution function of gas/vapor molecules. In MGD analyses, macroscopic values (density, velocity, temperature, etc.) at an arbitrary position and mass, momentum, and energy fluxes passing through an arbitrary surface in gas/vapor phases can be calculated by solving velocity distribution functions of molecules, which are governed by the Boltzmann equation.

Competing interests: The authors have declared that no competing interests exist.

In previous studies, bubble collapse [4, 5], droplet evaporation [6], and nanoporous evaporation [7] have been investigated via MGD analysis taking into consideration the evaporation and condensation of molecules at the interface. When investigating physical phenomena accompanied by evaporation/condensation in MGD analysis, we need to impose a boundary condition on the vapor–liquid interface that represents the evaporation and condensation of molecules. This boundary condition is called the kinetic boundary condition (KBC). Evaporation from the liquid phase and condensation into it cannot be accurately represented without KBCs and, therefore, setting them is indispensable for MGD analysis of phase change phenomena. Because the Boltzmann equation for MGD analyses governs the temporal and spatial evolutions of the velocity distribution function of gas/vapor molecules, the KBC also has the form of the velocity distribution function.

For the vapor molecules outgoing to the vapor phase from the liquid phase, the KBC is given by the following function [8]:

$$f_{\mathrm{out}} = \frac{\alpha_{\mathrm{e}}\rho^{*} + (1-\alpha_{\mathrm{c}})\sigma}{\left(\sqrt{2\pi R T_{\mathrm{L}}}\right)^{3}} \exp\left(-\frac{\xi_x^2+\xi_y^2+\xi_z^2}{2RT_{\mathrm{L}}}\right), \quad \text{for } \xi_z > 0, \tag{1}$$

where R is the gas constant of the vapor, T_{L} is the liquid temperature, ρ^{*} is the saturated vapor density at T_{L}, and σ is a parameter related to the density of molecules that collide with the vapor–liquid interface from the vapor phase. $\boldsymbol{\xi} = (\xi_x, \xi_y, \xi_z)$ denotes the molecular velocities along the x-, y-, and z-directions, where z is the direction normal to the liquid surface. σ is defined by

$$\sigma = -\sqrt{\frac{2\pi}{RT_{\mathrm{L}}}}\int_{-\infty}^{0}\int_{-\infty}^{\infty}\int_{-\infty}^{\infty}\xi_z f_{\mathrm{coll}}\, d\xi_x d\xi_y d\xi_z, \tag{2}$$

where f_{coll} is the velocity distribution function of the molecules having $\xi_z < 0$ at the vapor–liquid interface and colliding with the interface from the vapor phase. f_{coll} can be obtained by solving the Boltzmann equation in MGD analysis.

α_{e} and α_{c} in Eq 1 are the evaporation and condensation coefficients, and they have been widely defined as the ratio of mass fluxes of molecules [8–13] as follows:

$$\alpha_{\mathrm{e}} = \frac{J_{\mathrm{evap}}}{J_{\mathrm{out}}^{*}}, \quad \alpha_{\mathrm{c}} = \frac{J_{\mathrm{cond}}}{J_{\mathrm{coll}}}, \tag{3}$$

where J_{evap} is the mass flux of the evaporation molecules, J_{out}^{*} is the mass flux of the outgoing molecules from the liquid phase to the vapor phase in the vapor–liquid equilibrium state given by $J_{\mathrm{out}}^{*} = \rho^{*}\sqrt{RT_{\mathrm{L}}/2\pi}$, J_{cond} is the mass flux of the condensation molecules, and J_{coll} is the mass flux of the colliding molecules from the vapor phase to the liquid phase. In addition, there is the other mass flux J_{ref} of molecules that are reflected at the vapor–liquid interface and return to the vapor phase. The relationships between these fluxes defined in the vicinity of the vapor–liquid interface are shown in Fig 1a. The mass fluxes of the outgoing molecules, J_{out}, and the colliding molecules, J_{coll}, are defined as

$$J_{\mathrm{out}} = J_{\mathrm{evap}} + J_{\mathrm{ref}}, \quad J_{\mathrm{coll}} = J_{\mathrm{ref}} + J_{\mathrm{cond}}. \tag{4}$$

As shown in the above definitions, α_{e} and α_{c} indicate the evaporation rate and condensation rate of the molecules, respectively.

When constructing KBCs for MGD analyses, we need to obtain the molecular velocity distributions and mass fluxes as represented in Eqs 1–3. Because these values cannot be obtained

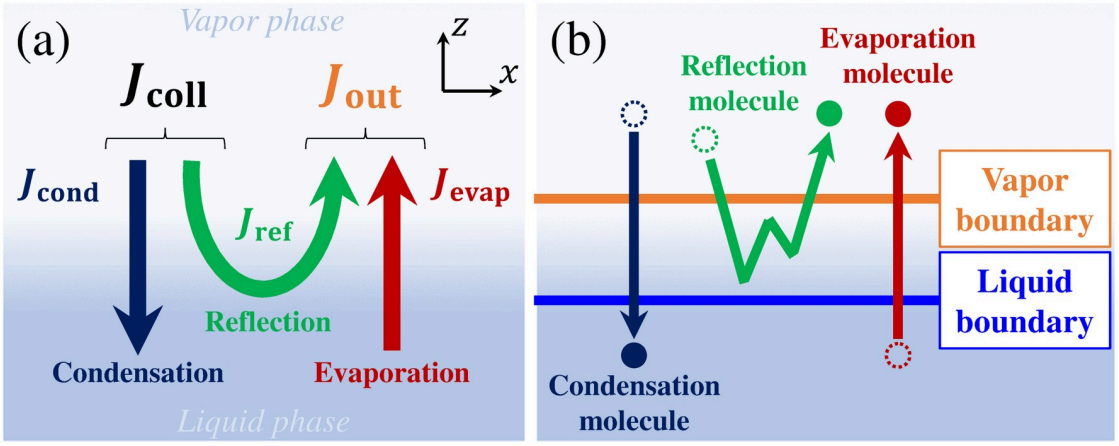

Fig 1. (a) Mass fluxes in the vicinity of vapor–liquid interface; (b) classification of molecules with vapor and liquid boundaries.

https://doi.org/10.1371/journal.pone.0248660.g001

from MGD analyses, it is necessary to conduct molecular-scale simulations that can analyze the motions of individual molecules in detail. In particular, the definitions of α_e and α_c make it necessary to classify molecules in the vicinity of the vapor–liquid interface into evaporation, reflection, and condensation molecules as represented in Eqs 3 and 4. Currently, several studies using the molecular dynamics (MD) simulation [9, 10, 12–20] or the Enskog–Vlasov direct simulation Monte Carlo (EV-DSMC) method [8, 11, 21–25] have been conducted to investigate evaporation and condensation from the standpoint of molecular motions. However, the classification criterion for molecules is not uniquely defined, because there is no clear definition of evaporation, reflection, and condensation of molecules. Thus, there have been various discussions on the method of classifying molecules, and several approaches to the construction of KBCs have been proposed in previous studies [8, 9, 11–15, 22, 24, 26].

For defining molecular motions and classifying molecules, a method that involves setting two imaginary boundaries, which was proposed by Meland et al. [15] and Gu et al. [26], has been utilized in some previous studies [12, 13, 15, 24, 26]. The relationship between the two imaginary boundaries—the liquid boundary and vapor boundary—and classified molecules is shown in Fig 1b. In this method, a molecule that passes two boundaries from the liquid phase to the vapor phase is defined as an evaporation molecule; a molecule that passes two boundaries from the vapor phase to the liquid phase is defined as a condensation molecule; a molecule that passes the vapor boundary from the vapor phase and returns to the vapor phase without passing the liquid boundary is defined as a reflection molecule. The molecules are classified according to the balance between their reaching positions and the set position of the boundaries as shown in Fig 1b. In our previous study, we applied this method in a multi-component system to construct the KBCs for vapor and non-condensable gas molecules [13]. Because the position of the vapor boundary is related to the position where the KBC is applied, the definition of the position of the vapor boundary has already been established from its relationship with the framework of MGD [8, 12, 27]. Hence, we set the vapor boundary at the position of the KBC. On the other hand, we had determined the position of the liquid boundary [12] such that the value of the mass flux of the evaporation molecules coincides with that in the virtual-vacuum condition proposed by Ishiyama et al. [9, 14].

In the classification method that involves setting the two boundaries, the molecules are classified only by their reaching position, and the time that molecules stayed in the vicinity of the vapor–liquid interface is not included in the classification criteria [12]. Molecules that return

to the vapor phase without passing through the liquid boundary are classified as the reflection molecules in this method, even if they stayed in the vicinity of the liquid surface for a long time. Thus, there is a possibility that molecules that should be classified as condensation molecules are classified as reflection molecules instead. We consider that, for a single component system, reflection molecules should be the molecules that return to the vapor phase with a short stay on the liquid-phase side and have little interaction with liquid molecules. Unless molecules are properly classified when constructing KBCs, accurate MGD analysis of phase change phenomena cannot be conducted. Thus, in this study, we discuss the validity of the set position of the liquid boundary applied in our previous studies [12, 13, 24] by introducing a new concept, the staying time of molecules, which represents the time they stay in the vicinity of the interface. We obtained molecular properties such as the reaching position and the staying time in MD simulations without setting the liquid boundary, and statistically processed them to understand the characteristics of the molecular motions in the vicinity of the vapor–liquid interface. Based on the distribution of the staying time of molecules that reached in the vicinity of the position where the liquid boundary was set in our previous studies, we investigated whether that position is reasonable for the classification of molecules. Moreover, we also conducted an investigation on the molecular characteristics from the standpoints of molecular velocity distributions and the reflection process of molecules. In particular, while considering the velocity distributions of the reflection molecules, we investigated the dependence of the condensation coefficient α_c on the molecular velocity at which molecules incident from the vapor phase to the liquid phase.

2 Method

2.1 System condition

We used argon as the liquid and vapor molecules. The calculation domain, which consisted of 12, 000 argon molecules, is shown in Fig 2a. The periodic boundary condition was imposed in all directions of the calculation system. The lengths of the calculation domain L_x, L_y, and L_z were 8.0, 8.0, and 17.5 nm, respectively.

For the intermolecular potential between argon molecules, we used the following 12-6 Lennard-Jones potential function:

$$\phi_{\mathrm{Ar}}(r) = 4\varepsilon_{\mathrm{Ar}}\left[\left(\frac{\sigma_{\mathrm{Ar}}}{r}\right)^{12} - \left(\frac{\sigma_{\mathrm{Ar}}}{r}\right)^{6}\right], \tag{5}$$

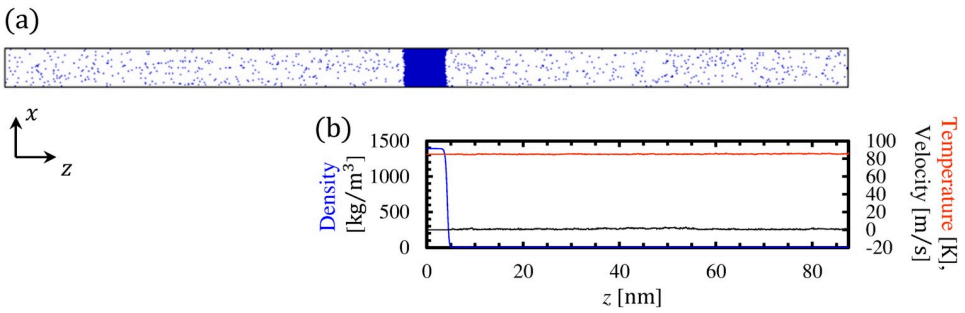

Fig 2. (a) Calculation system in the present MD study; (b) density, temperature, and velocity profiles in system.

https://doi.org/10.1371/journal.pone.0248660.g002

where the molecular diameter σ_{Ar} is 0.3405 nm, the potential depth ε_{Ar} is 1.635×10^{-21} J, and r is the distance between two molecules. The cutoff radius was set to 1.5 nm, and the Newton's law of motion was solved by the leapfrog method with time step $\Delta t = 5$ fs.

To establish the equilibrium state for the initial condition of this MD study, we conducted the equilibrium calculation with a temperature control [28] applied to the argon molecules. In the process of this equilibrium calculation, we applied the velocity scaling method at the desired temperature $T = 85$ K. To confirm that the system had reached the equilibrium state, we calculated the density, temperature, and velocity profiles in the system as shown in Fig 2b. These macroscopic values were calculated from the averages for the equilibrium calculation over 200 ns in control volumes with dimensions $L_x \times L_y \times \Delta z$, where $\Delta z = 0.1$ nm. Here, the velocity profile is derived from the sum of x-, y-, and z-directional average velocities of molecules. Because the calculation system is symmetric about $z = 0$, the macroscopic values in Fig 2b are obtained by averaging the values on the left ($z \leq 0$) and right ($z > 0$) parts. We can confirm that the average velocity became 0 m/s and the average temperature became 85 K throughout the calculation system. We have also confirmed that a sum of potential energy of molecules has converged, and since the temperature and velocity profiles are uniform throughout the system, we concluded that it has reached the vapor–liquid equilibrium state at $T = 85$ K. Using this vapor–liquid equilibrium system as the initial condition, we conducted the main simulations for the present study without applying the temperature control.

2.2 Definitions of molecular variables

In this study, we needed to obtain variables that characterize molecular motions without setting the liquid boundary whose definition is ambiguous. To obtain them, we only set the vapor boundary at the position of the KBC. Here, molecular variables in this study refer to values that can be obtained from molecules based on the position of the vapor boundary. For instance, they include the staying time of molecules which represents a time that a molecule stayed on the liquid-phase side of the vapor boundary (Fig 3). Before giving detailed definitions of molecular variables, we describe the position of the KBC where the vapor boundary is applied.

When specifying the position of the KBC, the following normalized z coordinate is commonly utilized:

$$\bar{z} = \frac{z - \mathrm{Z_m}}{\delta}, \tag{6}$$

where δ is the 10–90 thickness of the density transition layer, and Z_m is the position of the center of this transition layer. These values were obtained from the hyperbolic tangent function [9, 29] given by

$$\rho(z) = \frac{\rho_v + \rho_l}{2} + \frac{\rho_v - \rho_l}{2} \tanh\left(\frac{z - \mathrm{Z_m}}{0.455\delta}\right), \tag{7}$$

where ρ_v and ρ_l are the densities in the bulk vapor and liquid phases, respectively. In this study, δ became 0.765 nm and Z_m became 4.24 nm from fitting Eq 7 to the density profile in Fig 2b. We set the vapor boundary at $\bar{z} = 3.0$, where the KBCs are widely applied [27].

We obtained variables from the molecules that passed through the vapor boundary toward the liquid phase and passed through the boundary again to return to the vapor phase as shown in Fig 3, because we set only the vapor boundary in this study. From the position of the vapor boundary, we obtained the reaching position z_{reach} and the staying time t_{stay}. The reaching position z_{reach} was defined as the minimum value of $\bar{z}$ that a molecule had reached, and the staying time t_{stay} was defined as the time that a molecule had stayed on the liquid-phase side of

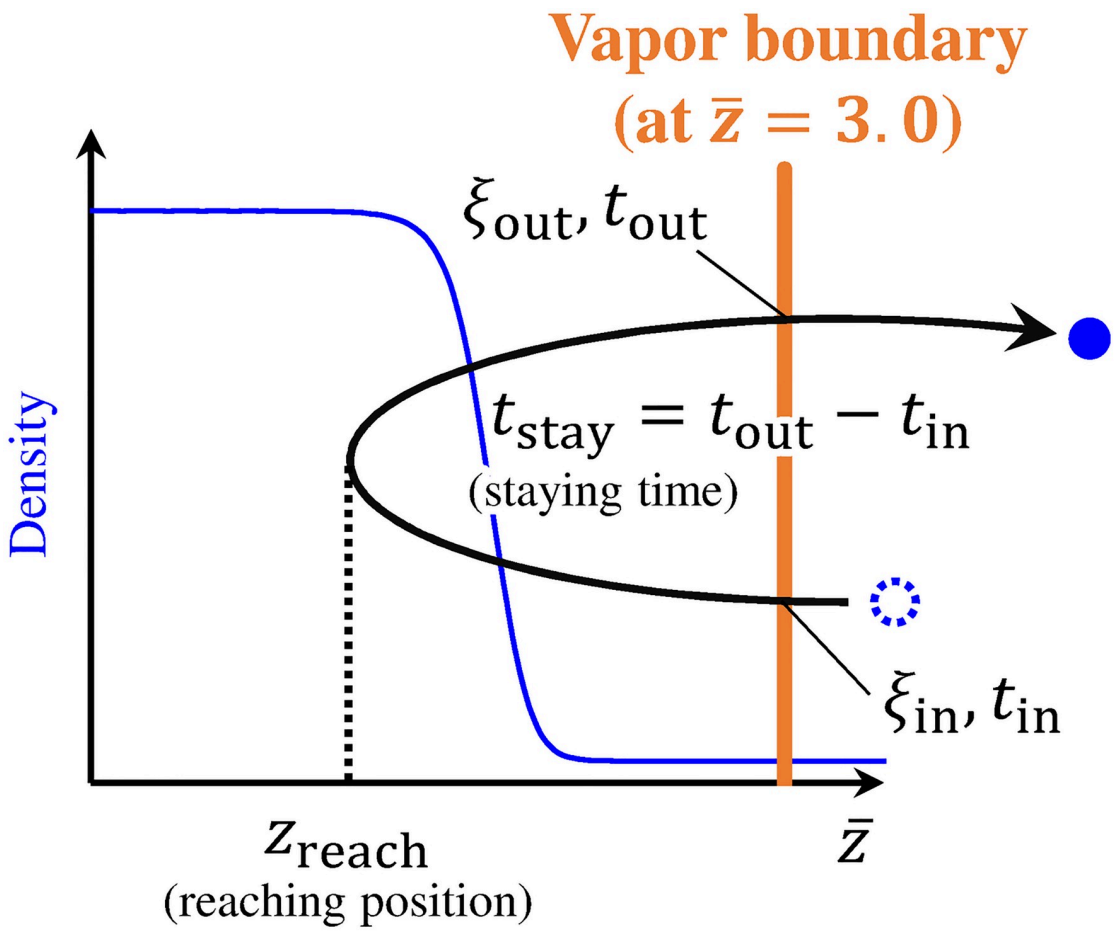

Fig 3. Schematic of method to obtain molecular variables. Reaching position z_{reach} was defined as the minimum value of $\bar{z}$ that the molecule had reached; staying time t_{stay} was defined as the time that the molecule had stayed in the region on the liquid-phase side of the vapor boundary; ξ_{in} and ξ_{out} were molecular velocities along the z-direction when the molecule passed through the vapor boundary toward the liquid phase and vapor phase, respectively.

https://doi.org/10.1371/journal.pone.0248660.g003

the vapor boundary. In addition to z_{reach} and t_{stay}, we also defined the incident velocity ξ_{in} and outgoing velocity ξ_{out} as the molecular velocities normal to the vapor boundary (the molecular velocities along the z-direction). ξ_{in} and ξ_{out} were the velocities when a molecule passed through the vapor boundary toward the liquid phase ($\xi_{in} < 0.0$) and toward the vapor phase ($\xi_{out} > 0.0$), respectively. In regard to the condensation and molecular motion, it has been reported that the condensation coefficient of monatomic molecules depends on their translational energy in the direction normal to the liquid surface [30]. Thus, ξ_{in} and ξ_{out} in this study were defined as the molecular velocities normal to the vapor boundary, and we used them for the investigation of a relationship between z-directional velocities of molecules and their condensation or reflection process.

When a molecule returned to the vapor phase, z_{reach}, t_{stay}, ξ_{in}, and ξ_{out} were recorded at the same time as samples of the molecule. To obtain a sufficient number of samples of z_{reach}, t_{stay}, ξ_{in}, and ξ_{out}, we performed the MD simulation in the equilibrium state, in which molecules constantly move toward and away from the vapor–liquid interface. The sampling number of molecules in this study was 100, 000 in all. Because we have confirmed that almost the same

results can be obtained when the sampling number of molecules is 10,000, we consider that 100,000 is a sufficient number for the investigation in this study.

Because we had set the liquid boundary at $\bar{z} \approx -1.0$ in our previous studies [12, 13, 24], we will discuss the validity of this position based on the balance between the variables z_{reach} and t_{stay} of molecules. In particular, we classified the molecules using data clustering as one classification model depending on the two variables z_{reach} and t_{stay} to verify whether the method that involved setting the two boundaries, which classifies molecules depending only on their reaching position, is a reasonable classification method. We used the *k*-means method of the partitional algorithm for the classification of a dataset [31–33] because it is one of the most popular and the simplest algorithms [34]. The details of the *k*-means method are described in the S1 Appendix. By using data clustering, we can classify a dataset into clusters according to the similarity of the properties of the data points in the dataset. In other words, molecules were classified into clusters based on the similarity of the molecular variables z_{reach} and t_{stay} using the *k*-means method of data clustering. Owing to the method used to obtain the molecular variables shown in Fig 3, we classified the molecules into two types: molecules with shorter staying times and larger reaching positions, and molecules with longer staying times and smaller reaching positions. From the characteristics of each type of molecules, we considered that the former molecules got reflected and that the latter molecules had condensed once and then evaporated. Thus, we defined the former molecules as reflection molecules and the latter molecules as condensation/evaporation molecules in this study. We classified molecules into reflection molecules and condensation/evaporation molecules by the *k*-means method that includes both z_{reach} and t_{stay} as variables for clustering. In accordance with the relationship between the variables z_{reach} and t_{stay} of the molecules and the results of the *k*-means method applied to these variables, we organized the molecular motions in the vicinity of the vapor–liquid interface, and investigated the validity of the position of the liquid boundary at $\bar{z} \approx -1.0$.

3 Results and discussion

3.1 Reaching position and staying time of molecules

We first describe the features of the dataset representing the relationship between the z_{reach} and t_{stay} of molecules. Subsequently, we show the results of the *k*-means method that classified molecules into reflection molecules and condensation/evaporation molecules as a model of classification that depends on the two variables z_{reach} and t_{stay}.

Fig 4a shows the dataset representing the relationship between the z_{reach} and t_{stay} of the molecules. A data point in this figure denotes the z_{reach} and t_{stay} of a molecule. Because we aimed to classify molecules in the vicinity of the vapor–liquid interface, we excluded the data points of molecules that reached the deeper bulk liquid phase. To align the distance from the center of the transition layer of the vapor–liquid interface located at $\bar{z} = 0.0$, we show the data points of molecules whose z_{reach} values were in the range $-3.0 < \bar{z} < 3.0$ in Fig 4a. The remaining number of data points is 71, 319 out of 100, 000. This figure shows that the molecules that did not pass through the vapor–liquid interface (the molecules with $0.0 < z_{\mathrm{reach}} < 3.0$) returned with a short staying time t_{stay}. This indicates that t_{stay} did not increase when the molecules were reflected in the vapor phase. On the contrary, there is a large variation in the distribution of the t_{stay} of molecules whose z_{reach} values were within $z_{\mathrm{reach}} < 0.0$. This means that t_{stay} tends to increase when molecules pass through the vapor–liquid interface and reach the liquid phase. The average t_{stay} values of molecules with $z_{\mathrm{reach}} \geq 0.0$ and $z_{\mathrm{reach}} < 0.0$ are approximately 25.8 ps and 7.40×10^2 ps, respectively. We consider that this significant increase in t_{stay} was due to condensation into the liquid phase. From the variation in t_{stay} shown in Fig 4a, we can

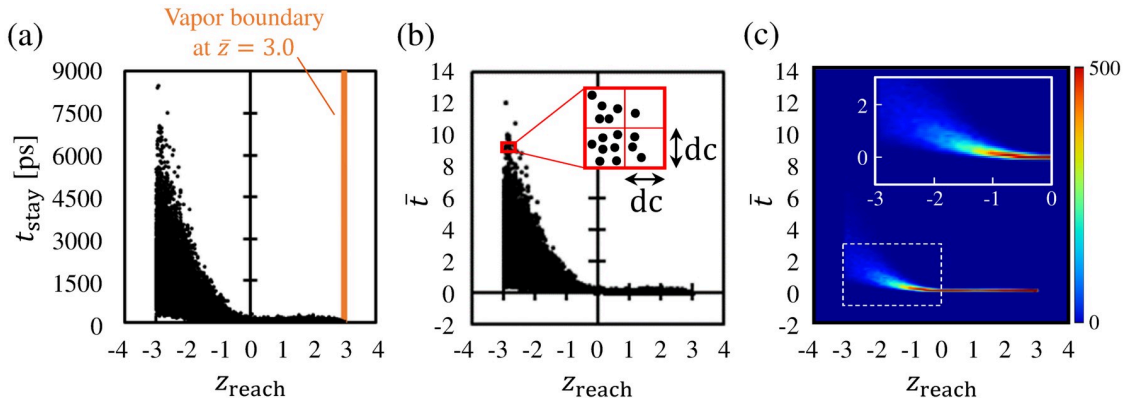

Fig 4. Relationship between z_{reach} and t_{stay} of molecules in $-3.0 < z_{reach} < 3.0$. (a) Dataset representing relationship between z_{reach} and t_{stay} of molecules; (b) dataset in z_{reach}–$\bar{t}$ coordinate plane. Bins with dc × dc are set to calculate the values of the bivariate histogram. (c) Bivariate histogram of data points in z_{reach}–$\bar{t}$ coordinate plane.

https://doi.org/10.1371/journal.pone.0248660.g004

confirm that the tendency of the t_{stay} of molecules changes depending on whether the molecules passed through the vapor–liquid interface.

Although Fig 4a shows the outline of the variation in the data points, the distribution of the number of data points in this figure is unclear. Thus, we constructed the bivariate histogram of the data points in this dataset. We set bins with dc × dc as shown in Fig 4b to count the numbers of data points for the construction of the histogram. To approximately unify the scales of dc in the t_{stay} and z_{reach} directions, we introduced the non-dimensional $\bar{t}$ coordinate given by

$$\bar{t} = \frac{t_{stay}}{\mu_t}, \tag{8}$$

where $\mu_t = 6.99 \times 10^2$ ps is the standard deviation of t_{stay}. This μ_t was derived from the t_{stay} of molecules whose z_{reach} values were within $-3.0 < z_{reach} < 3.0$. We utilized the z_{reach}–$\bar{t}$ coordinate plane shown in Fig 4b to construct the histogram, and we set dc to 0.1 (to form a balance between the resolution of the histogram and the number of data points). Fig 4c shows the bivariate histogram of data points in the z_{reach}–$\bar{t}$ coordinate plane. The histogram is represented as the gradation image, and the inset of Fig 4c shows the region surrounded by the dotted rectangle. The color bar denotes number of data points in each bin. As shown in Fig 4c, the bivariate histogram exhibits higher values in $0.0 < z_{reach} < 3.0$, which is the region between the vapor–liquid interface and the vapor boundary, and it exhibits quite small values in $z_{reach} < -2.0$, which is the region inside the bulk liquid phase. In addition, we can confirm that the values in the bivariate histogram gradually change in the region $-2.0 < z_{reach} < 0.0$. This means that the molecular characteristic in the relationship between z_{reach} and t_{stay} changes around $-2.0 < z_{reach} < 0.0$, which is the region in the liquid-phase side of the vapor–liquid interface. We consider that this result supports the validity of setting the liquid boundary for the classification of molecules somewhere within this range.

We next show a classification model depending on the two variables z_{reach} and t_{stay} yielded by the *k*-means method. The dataset is classified into clusters according to the position of the centroids of data points by the *k*-means method. For details about this method, see the S1 Appendix. The results from the *k*-means method for classifying the molecules into two clusters is shown in Fig 5a. In this figure, the molecules are classified into two clusters: (1) a cluster of molecules with shorter t_{stay} and larger z_{reach} represented by the blue dots, and (2) a cluster of molecules with longer t_{stay} and smaller z_{reach} represented by the orange dots. From the

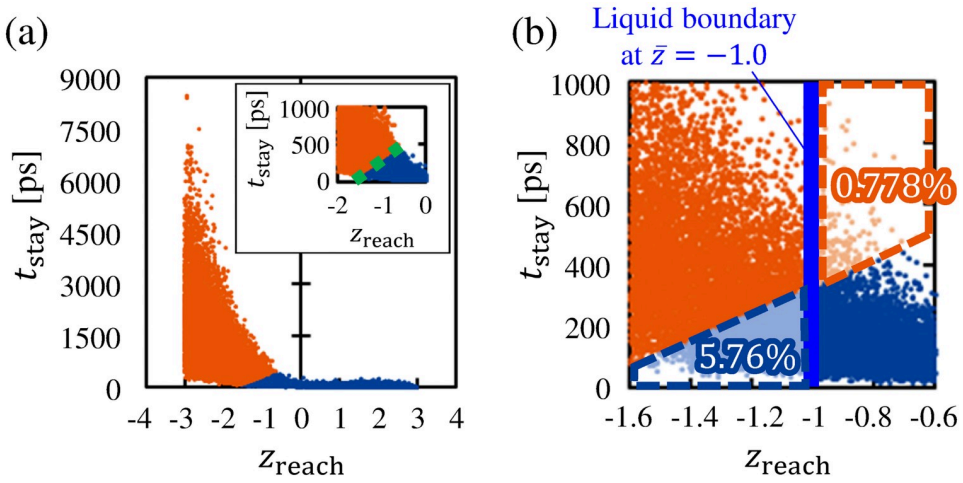

Fig 5. Results of *k*-means method. (a) Dataset classified into two clusters. Blue dots represent the cluster of reflection molecules, and orange dots represent the cluster of condensation/evaporation molecules. Inset shows that the two clusters are divided by a dotted line at approximately $z_{reach} = -1.0$. (b) Percentages of excluded molecules from each cluster in the case where the liquid boundary was set at $\bar{z} = -1.0$.

https://doi.org/10.1371/journal.pone.0248660.g005

characteristics of each cluster, the former was defined as the cluster of the reflection molecules, and the latter was defined as the cluster of condensation/evaporation molecules, as explained in the "Method" section. The numbers of the reflection molecules and condensation/evaporation molecules in this figure are 44, 727 and 26, 592, respectively. The inset of Fig 5a shows the region $-2.0 < z_{reach} < 0.0$, which is the vicinity of the boundary between the two clusters, and the dotted line demarcates the boundary between them. Fig 5a and its inset indicate that the molecules were divided into two clusters at approximately $z_{reach} = -1.0$. To be specific, the dotted line, which represents the boundary between the two clusters, has a slope in approximately the range of $-1.5 < z_{reach} < -0.5$. Most of the range where the bivariate histogram of Fig 4c takes high values is composed of reflection molecules, and their average t_{stay} and that of the condensation/evaporation molecules are approximately 52.0 ps and 1.04×10^3 ps, respectively. Because the dataset is classified according to the position of the centroids of the data points in the *k*-means method, the slope of the dotted line in the inset of Fig 5a was caused by the large difference in the t_{stay} component of the centroids of the two clusters.

The molecules were classified on the basis of the two variables z_{reach} and t_{stay} in the *k*-means method, unlike the classification method that involves setting the two boundaries. To compare the classification results obtained from the *k*-means method and the method that involves setting the two boundaries (vapor and liquid boundaries), we calculated the difference in the numbers of molecules classified by the two classification methods. As we conduct the analysis about the liquid boundary set at $\bar{z} \approx -1.0$, we show the case where the liquid boundary is set at $\bar{z} = -1.0$. Fig 5b shows the percentages of molecules excluded by the liquid boundary from the clusters to which they originally belonged. As shown in this figure, approximately 5.76% of the reflection molecules and approximately 0.778% of the condensation/evaporation molecules are excluded from each cluster. Although there are some differences in the resulting classifications, the *k*-means method yielded a similar classification as that produced by the method that involved setting the two boundaries utilized in previous studies. From this result, we consider that it is not necessary to include t_{stay} in the classification criteria, if most of the molecules with short t_{stay} are classified as the reflection molecules by the liquid boundary set at $\bar{z} = -1.0$.

3.2 Staying time and position of liquid boundary

As discussed earlier, the bivariate histogram shown in Fig 4c and the clustering result shown in Fig 5 indicate some validity of the setting of the liquid boundary at $\bar{z} = -1.0$. In this subsection, we investigate the distribution of t_{stay} of molecules with $z_{reach} \leq -1.0$ and $z_{reach} > -1.0$ to confirm whether molecules with short t_{stay} are appropriately classified as reflection molecules when the liquid boundary is set at $\bar{z} = -1.0$.

Fig 6a shows the dataset for z_{reach} and t_{stay} within the ranges $-2.0 \leq z_{reach} \leq 0.0$ and $0 \text{ ps} \leq t_{stay} \leq 1000$ ps. The molecules with $-2.0 \leq z_{reach} \leq -1.0$ and $-1.0 < z_{reach} \leq 0.0$ are represented by the orange dots and blue dots, respectively. The distribution of the t_{stay} of these molecules is shown in Fig 6b, and the inset of Fig 6b shows the distribution of t_{stay} in $t_{stay} \leq 100$ ps. The cumulative bar graphs with the time interval $\Delta t_{stay} = 20$ ps denote the sum of the normalized numbers of molecules in the two z_{reach} ranges. The numbers of molecules are normalized by 25, 366, which is the total number of molecules with $-2.0 \leq z_{reach} \leq 0.0$. Fig 6a and 6b show that many of the molecules with $-1.0 < z_{reach} \leq 0.0$ had t_{stay} in the range around $t_{stay} < 200$ ps, whereas the molecules with $-2.0 \leq z_{reach} \leq -1.0$ had a widely distributed t_{stay} around $t_{stay} > 100$ ps. We can also confirm that there is a peak in the short t_{stay} range around $t_{stay} < 60$ ps. Here, it takes approximately 32.6 ps for a molecule to reciprocate the range $-1.0 < \bar{z} < 3.0$ at

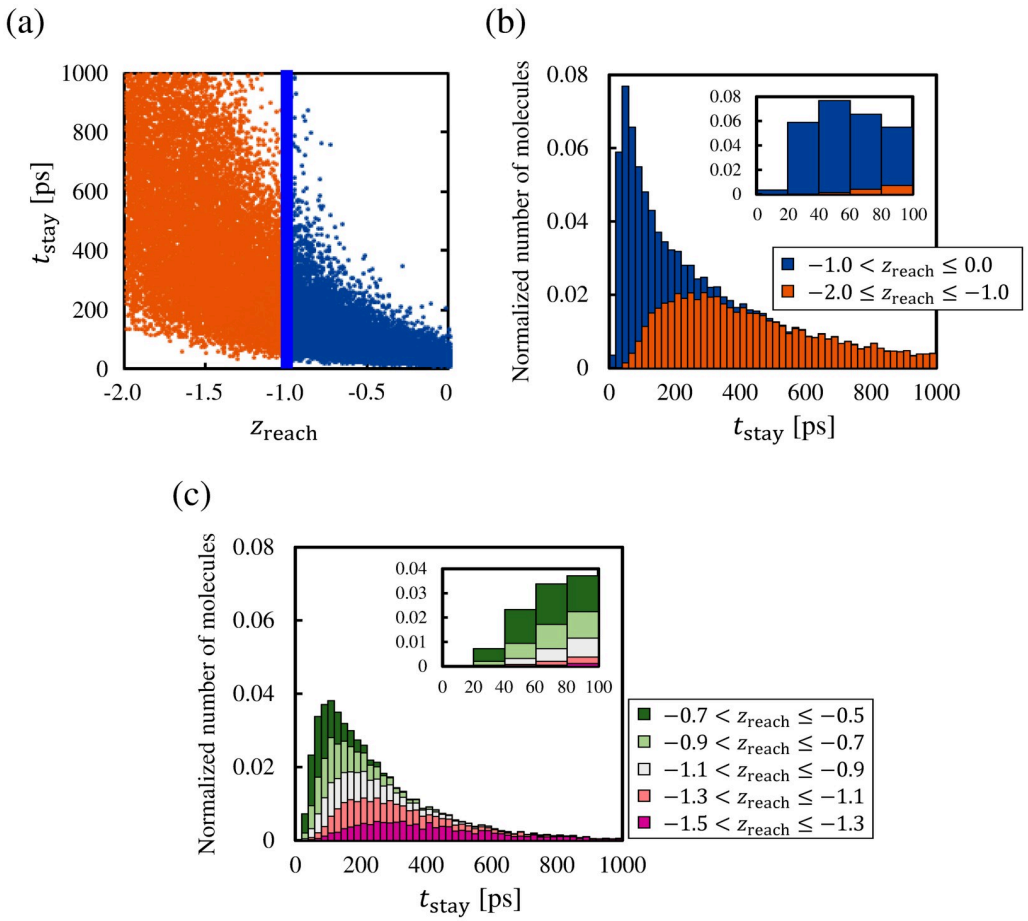

Fig 6. (a) Data points in $-2.0 \leq z_{reach} \leq 0.0$ and $0 \text{ ps} \leq t_{stay} \leq 1000$ ps. (b) Distribution of t_{stay} of molecules with $-2.0 \leq z_{reach} \leq 0.0$. (c) Distribution of t_{stay} of molecules with $-1.5 < z_{reach} \leq -0.5$. Bar graphs with the time interval 20 ps are composed of the normalized number of molecules in each range of z_{reach}.

https://doi.org/10.1371/journal.pone.0248660.g006

the most probable speed $\sqrt{2RT_L}$ of the Maxwellian, and the order of this time coincides with t_{stay} around the peak in the distribution of Fig 6b. Thus, we consider that the molecules with t_{stay} less than 100 ps should be classified as reflection molecules because of their early return to the vapor phase. From Fig 6b and its inset, we can see that the molecules with $-1.0 < z_{reach} \leq 0.0$ occupy a large part of the range $t_{stay} < 100$ ps. In fact, approximately 95% of molecules with $t_{stay} < 100$ ps have the z_{reach} values within $-1.0 < z_{reach} \leq 0.0$. This indicate that most of the molecules with a fairly short t_{stay} are classified as reflection molecules when we classify the molecules based on whether their z_{reach} is less than −1.0, that is, by setting the liquid boundary at $\bar{z} = -1.0$. Thus, we conclude that $\bar{z} = -1.0$ applied in our previous studies is the reasonable position of the liquid boundary for the classification of molecules.

In addition, we investigate whether there is a more suitable position of the liquid boundary at around $\bar{z} = -1.0$. Fig 6c shows the distribution of t_{stay} of molecules with $-1.5 < z_{reach} \leq -0.5$. We divided this z_{reach} range into five, and the cumulative bar graphs with the time interval Δt_{stay} = 20 ps denote the sum of the normalized numbers of molecules in each z_{reach} range. The numbers of molecules are normalized by 25, 366, which is the total number of molecules with $-2.0 \leq z_{reach} \leq 0.0$. The inset of Fig 6c shows the distribution of t_{stay} in the range $t_{stay} \leq 100$ ps. As shown in Fig 6c, there is a non-negligible number of molecules with $-0.9 < z_{reach} \leq -0.5$ in the short t_{stay} range ($t_{stay} < 100$ ps). Approximately 91% of molecules with $t_{stay} < 100$ ps have the z_{reach} values within $-0.9 < z_{reach} \leq 0.0$, and it indicates that almost the same classification as when the liquid boundary is set at $\bar{z} = -1.0$ can be obtained by setting the liquid boundary at $\bar{z} = -0.9$. From the above results, we found that most of the molecules with a fairly short staying time ($t_{stay} < 100$ ps) are classified as reflection molecules when the liquid boundary is set at $\bar{z} = -0.9$ or −1.0. Therefore, we conclude that the suitable position of the liquid boundary for the classification of molecules is $-1.0 \leq \bar{z} \leq -0.9$.

3.3 Incident and outgoing velocities of reflection molecules

In this subsection, we investigate the characteristics of reflection molecules in terms of their incident and outgoing velocities. From this subsection, we define the molecules with $z_{reach} \leq -1.0$ as condensation/evaporation molecules and those with $-1.0 < z_{reach} < 3.0$ as reflection molecules. The numbers of reflection molecules and condensation/evaporation molecules according to this definition are 42, 359 and 57, 641, respectively. The dataset representing the relationship between the incident velocity and the outgoing velocity of reflection molecules is shown in Fig 7a. ζ_{in} in the abscissa and ζ_{out} in the ordinate are the normalized molecular velocities $\zeta_{in} = |\xi_{in}|/\sqrt{2RT_L}$ and $\zeta_{out} = \xi_{out}/\sqrt{2RT_L}$, respectively. $\sqrt{2RT_L}$ denotes the most probable speed of the Maxwellian at the liquid temperature T_L = 85 K. The incident velocity ξ_{in}, which was in the negative z-direction as shown in Fig 3, was set to be positive for comparison with the outgoing velocity ζ_{out} in the same coordinate system. To investigate the distribution of the data points, we constructed the bivariate histogram of this dataset as shown in Fig 7b. The bivariate histogram in the ζ_{in}–ζ_{out} coordinate plane is constructed and represented using the same method that involves setting the bins with dc × dc = 0.1 × 0.1 as in Fig 4c. We can confirm that the bivariate histogram shows the high values in the ranges $0 < \zeta_{in} < 1.0$ and $0 < \zeta_{out} < 1.0$ in Fig 7b. Approximately 64% of reflection molecules had the incident and outgoing velocities in these velocity ranges, and it means that they had lower ζ_{in} and ζ_{out} than the most probable speed of the Maxwellian ζ_z = 1.0.

Fig 7c shows the velocity distribution functions for the incident and outgoing velocities of the reflection molecules. The velocity distributions in this figure are shown as functions of $\zeta_z \hat{f}_{in}$ and $\zeta_z \hat{f}_{out}$, where $\hat{f}_{in}$ and $\hat{f}_{out}$ are the normalized velocity distribution functions of the incident velocity and outgoing velocity, respectively. The solid line represents the normalized

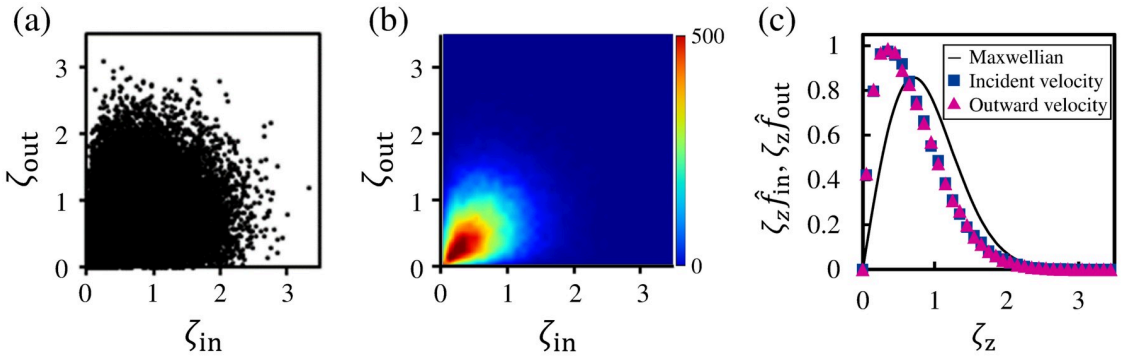

Fig 7. Relationship between normalized molecular velocities ζ_{in} and ζ_{out} of reflection molecules. (a) Data points representing the relationship between ζ_{in} and ζ_{out} of reflection molecules. Sampling number of reflection molecules is 42, 359. (b) Bivariate histogram in the ζ_{in}–ζ_{out} coordinate plane. (c) Molecular velocity distribution functions of reflection molecules for the normalized incident velocity ζ_{in} and normalized outgoing velocity ζ_{out}.

https://doi.org/10.1371/journal.pone.0248660.g007

Maxwellian at 85 K given by $\zeta_z \hat{f}^* = 2\zeta_z \exp(-\zeta_z^2)$, where $\hat{f}^*$ is the normalized velocity distribution function of molecules in the vapor–liquid equilibrium state. As shown in Fig 7c, the incident and outgoing velocities show almost the same velocity distribution functions. Fig 7c also indicates that the velocity distribution functions of $\zeta_z \hat{f}_{in}$ and $\zeta_z \hat{f}_{out}$ exhibit large deviations from the Maxwellian. The peaks of these distributions are formed at approximately $\zeta_z = 0.4$, which is a smaller velocity than the mean velocity of the Maxwellian, $\zeta_m \approx 0.707$. This means that in the velocity distributions of reflection molecules, the ratio of molecules with low velocities is higher than that in the Maxwellian. Therefore, it can be said that molecules with a low incident velocity are easily reflected. In addition, from the deviation of the velocity distribution function for the outgoing velocity from the Maxwellian, we can confirm that many of the reflection molecules pass through the vapor boundary toward the vapor phase without being accelerated to their z-directional velocity after reflection.

Basically, the velocity distribution function of all incident molecules follows the Maxwellian in the vapor–liquid equilibrium state. The reflection of molecules with a lower incident velocity indicates the possibility that molecules with a higher incident velocity will reach the liquid phase. Therefore, we next investigate the relationship between the reaching position z_{reach} and the incident velocity ξ_{in} of molecules.

3.4 Reaching position and incident velocity

The dataset representing the relationship between z_{reach} and the normalized incident velocity ζ_{in} of molecules is shown in Fig 8a, and the bivariate histogram of this dataset is shown in Fig 8b. The bivariate histogram is constructed using the same method that involves setting the bins with dc × dc = 0.1 × 0.1 as in Fig 4c. Although we excluded the data points of molecules with $z_{reach} < -3.0$ in the previous subsections, the data points of all sample molecules, including the molecules with $z_{reach} \leq -3.0$ that reached the deep bulk liquid phase, are shown in these figures for elucidating the dependence of the z_{reach} of molecules on their incident velocities. Thus, the sample number of molecules in Fig 8 is 100, 000. As shown in Fig 8b, many of the molecules with a low incident velocity were reflected in the vicinity of the vapor boundary at $\bar{z} = 3.0$. The average incident velocity of molecules whose z_{reach} values were within $2.0 < z_{reach} < 3.0$ is $\zeta_{in} = 0.459$, and it indicates that molecules with low incident velocities promptly return to the vapor phase. Furthermore, approximately 65% of the molecules with $\zeta_{in} > 0.5$

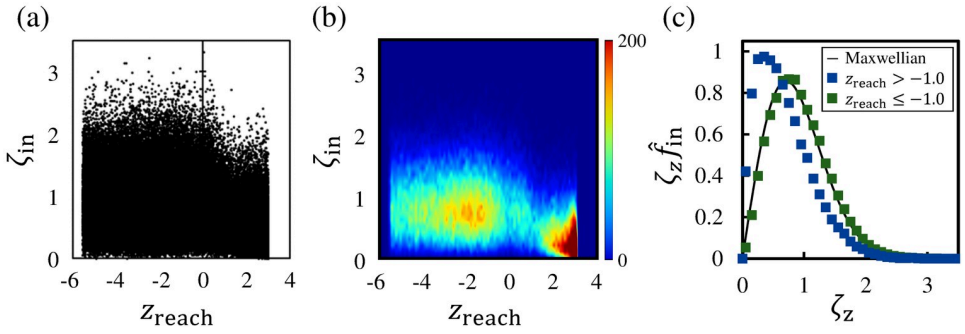

Fig 8. Relationship between z_{reach} and normalized incident velocity ζ_{in} of molecules. (a) Data points representing the relationship between z_{reach} and ζ_{in} of all sampling molecules. (b) Bivariate histogram in the z_{reach}–ζ_{in} coordinate plane. (c) Molecular velocity distribution functions of reflection molecules whose z_{reach} values lie in $z_{reach} > -1.0$ and condensation/evaporation molecules whose z_{reach} values lie in $z_{reach} \leq -1.0$.

https://doi.org/10.1371/journal.pone.0248660.g008

had z_{reach} values within $z_{reach} \leq -1.0$, and it means that many of the molecules with not so low ζ_{in} are easy to reach the liquid phase and condense into it.

We next compare the incident velocity of the reflection molecules and that of the condensation/evaporation molecules using the velocity distribution functions. Fig 8c shows the velocity distribution functions for the incident velocity of the reflection molecules with $z_{reach} > -1.0$ and the condensation/evaporation molecules with $z_{reach} \leq -1.0$. As in Fig 7c, the velocity distribution functions are shown as a function of $\zeta_z \hat{f}_{in}$. The solid line represents the Maxwellian at 85 K given by $\zeta_z \hat{f}^*$, and the velocity distribution function of the reflection molecules in Fig 8c is identical to that in Fig 7c. As shown in Fig 8c, the velocity distribution function of the condensation/evaporation molecules is almost consistent with the Maxwellian, unlike that of the reflection molecules. The incident velocity in the region where the bivariate histogram shows the higher values in $\bar{z} < -1.0$ in Fig 8b corresponds to the mean velocity of the Maxwellian. This means that the molecules basically reach $\bar{z} < -1.0$ and condense into the liquid phase when their incident velocities are nearly equal to the mean velocity of the Maxwellian. Fig 8 demonstrates that the incident velocity greatly influences the reaching position z_{reach}, i.e., the condensability of molecules, and we conclude that the condensation of molecules depends on their incident velocity. However, the dependence of the condensation coefficient α_c, which is defined as the ratio of the molecular mass fluxes, on the incident velocity of molecules has not been investigated. Thus, in the next subsection, we discuss α_c and its relationship with the molecular incident velocity.

3.5 Condensation coefficient and incident velocity

3.5.1 Dependence of condensation coefficient on incident velocity. We first show the relationship between α_c and molecular mass fluxes in detail. From Eqs 3 and 4, α_c is given by

$$\alpha_c = 1 - \frac{J_{ref}}{J_{coll}}. \tag{9}$$

We assume that the mass flux of colliding molecules J_{coll} in the vapor–liquid equilibrium state is given by

$$J_{coll} = -\int_{-\infty}^{0}\int_{-\infty}^{\infty}\int_{-\infty}^{\infty} \xi_z f^* \, d\xi_x d\xi_y d\xi_z = \rho^* \sqrt{\frac{RT_L}{2\pi}}, \tag{10}$$

where f^* is the Maxwellian at a liquid temperature T_L. Combining Eqs 9 and 10, we can

derive α_c as

$$\alpha_c = 1 - \frac{J_{ref}}{\rho^* \sqrt{RT_L/2\pi}}. \quad (11)$$

From this equation, we can calculate α_c from the mass flux J_{ref} and the saturated vapor density ρ^*. Fig 9a shows the time evolution of J_{ref} throughout the MD simulation in this study. The value of the mass flux reaches a certain constant value, although it fluctuates in the first stage of the simulation. From the time average of the value of the mass flux, we obtained $J_{ref} = 3.407$ g/cm^2 s. Further, the density field of the argon molecules in the calculation system shown in Fig 2 provided the saturated vapor density as $\rho^* = 4.761$ kg/m^3. This ρ^* is calculated from the average density in the region of the bulk vapor phase. From these values, we obtained α_c in the present MD simulation as $\alpha_c = 0.865$. This value of α_c agrees well with that calculated in the previous studies [10, 13]. Hence, we concluded that α_c in this study was correctly calculated from the J_{ref} obtained by this MD simulation and the J_{coll} obtained by Eq 10.

We next investigate α_c in detail using Eqs 10 and 11. As we discussed in the previous subsection, the molecules reflected in the vicinity of the vapor boundary had low incident velocities. Moreover, Fig 8b shows that many of the molecules whose incident velocities were nearly equal to the mean velocity of the Maxwellian reached and condensed into the liquid phase. These results represent that the condensability of molecules depends on their incident velocity at the liquid phase. In fact, it has been reported that the condensation coefficient shows the low value for the small molecular translational energy in the normal component to the liquid surface in the previous studies [30, 35, 36]. However, in these previous studies, the definitions of the condensation of molecules and the condensation coefficient were different from the definitions used in the present study. Hence, to confirm the dependency of α_c on the incident velocity of molecules based on the definition of the present study, we calculated α_c for each incident velocity range.

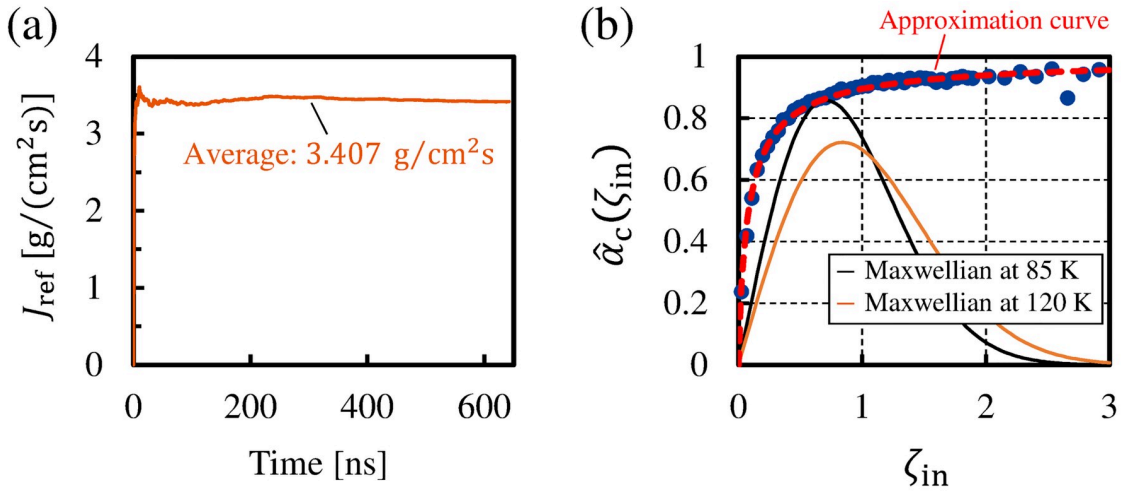

Fig 9. (a) Time evolution of J_{ref} in the present MD study; (b) condensation coefficient for each range of incident velocity ζ_{in}.

https://doi.org/10.1371/journal.pone.0248660.g009

From Eq 10, the mass flux of colliding molecules with an incident velocity within the range $A < \xi_z < B$ is given by

$$J_{\mathrm{coll}}^{A-B} = -\int_A^B \int_{-\infty}^{\infty} \int_{-\infty}^{\infty} \xi_z f^* \, d\xi_x d\xi_y d\xi_z, \ \text{for } B < 0. \tag{12}$$

The velocity interval $\Delta\xi_z$ for the calculation was set to $\Delta\xi_z = B - A = 8$ m/s. We also calculated J_{ref}^{A-B} from the incident velocities ξ_{in} of reflection molecules within the range $A < \xi_z < B$, which were obtained in the present MD simulation. By assigning J_{coll}^{A-B} and J_{ref}^{A-B} to Eq 9, the condensation coefficient $\hat{\alpha}_{\mathrm{c}}$ of molecules with incident velocities in $A < \xi_z < B$ is given by

$$\hat{\alpha}_{\mathrm{c}} = 1 - \frac{J_{\mathrm{ref}}^{A-B}}{J_{\mathrm{coll}}^{A-B}}. \tag{13}$$

Fig 9b shows $\hat{\alpha}_{\mathrm{c}}$ for each range of the normalized incident velocity ζ_{in}. The condensation coefficient is found to be a function of the molecular incident velocity $\hat{\alpha}_{\mathrm{c}}(\zeta_{\mathrm{in}})$ from this figure. We can see that the value of $\hat{\alpha}_{\mathrm{c}}(\zeta_{\mathrm{in}})$ increases as ζ_{in} increases, and $\hat{\alpha}_{\mathrm{c}}(\zeta_{\mathrm{in}})$ sensitively responds to ζ_{in} when ζ_{in} is less than the most probable speed in the Maxwellian ($\zeta_{\mathrm{in}} < 1.0$). This figure also shows that $\hat{\alpha}_{\mathrm{c}}(\zeta_{\mathrm{in}})$ becomes almost constant when $\zeta_{\mathrm{in}} < 1.0$ although $\hat{\alpha}_{\mathrm{c}}(\zeta_{\mathrm{in}})$ with $\zeta_{\mathrm{in}} > 2.0$ fluctuate due to the small number of sample molecules. The molecules with low ζ_{in} show a small value of $\hat{\alpha}_{\mathrm{c}}(\zeta_{\mathrm{in}})$, and it means that they are less likely to condense into the liquid phase than molecules with high ζ_{in}.

The dashed line in Fig 9b, which represents the approximation curve for $\hat{\alpha}_{\mathrm{c}}$, is given by

$$\hat{\alpha}_{\mathrm{c}}(\zeta_{\mathrm{in}}) = -\frac{C_1}{C_1 + \zeta_{\mathrm{in}}^{C_2}} + 1, \tag{14}$$

where $C_1 = 10.36$ and $C_2 = 0.8566$ under the conditions of the present MD simulation. Because this approximation curve is in good agreement with $\hat{\alpha}_{\mathrm{c}}$ obtained from Eq 13, the condensation coefficient as the function of ζ_{in} can be given by Eq 14 in this study.

Here, we show the relationship between α_{c} defined in Eq 11 and $\hat{\alpha}_{\mathrm{c}}(\zeta_{\mathrm{in}})$ defined in Eq 13. As shown in Fig 9b, $\hat{\alpha}_{\mathrm{c}}(\zeta_{\mathrm{in}})$ is the condensation coefficient of the function of the incident velocity. On the other hand, α_{c} defined in Eq 11 is the condensation coefficient of the entire incident velocity range $-\infty < \zeta_{\mathrm{in}} < 0$. Thus, by using $\hat{\alpha}_{\mathrm{c}}(\zeta_{\mathrm{in}})$, α_{c} is derived as

$$\alpha_{\mathrm{c}} = -\int_{-\infty}^{0} \zeta_z \hat{f}_{\mathrm{in}} \hat{\alpha}_{\mathrm{c}}(\zeta_z) \, d\zeta_z. \tag{15}$$

We have confirmed that α_{c} was calculated as $\alpha_{\mathrm{c}} = 0.864$ from this equation, and this value agrees well with the value of $\alpha_{\mathrm{c}} = 0.865$ calculated from Eq 11. Thus, we conclude that α_{c} was appropriately yielded by Eq 15 with $\hat{\alpha}_{\mathrm{c}}(\zeta_{\mathrm{in}})$ in Fig 9b.

3.5.2 Condensation coefficient in equilibrium state and non-equilibrium state. As defined in Eq 13, $\hat{\alpha}_{\mathrm{c}}(\zeta_{\mathrm{in}})$ was derived from J_{coll}^{A-B} and J_{ref}^{A-B}, which represent the mass fluxes of the colliding molecules and reflection molecules whose incident velocities were in certain ranges. Because the ratios between these fluxes are uniquely determined by the liquid temperature, the same profile of $\hat{\alpha}_{\mathrm{c}}(\zeta_{\mathrm{in}})$ as in Fig 9b will be obtained regardless of whether the calculation system is the non-equilibrium or equilibrium state when the liquid temperature is fixed as $T_{\mathrm{L}} = 85$ K. The molecular velocity distribution function for the incident velocity $\hat{f}_{\mathrm{in}}$ changes depending on the system state whereas $\hat{\alpha}_{\mathrm{c}}(\zeta_{\mathrm{in}})$ maintains the same profile in any state with $T_{\mathrm{L}} = 85$ K. This means that we can calculate α_{c} in the non-equilibrium state with $T_{\mathrm{L}} = 85$ K from $\hat{\alpha}_{\mathrm{c}}(\zeta_{\mathrm{in}})$ in Fig 9b and the molecular velocity distribution functions that depend on the

system state. Discussions on the relationship between molecular velocity distribution functions and the condensability based on the different definition from that in the present sutudy have been conducted in the previous study [36]. Thus, we next calculate α_c in the non-equilibrium state with the fixed liquid temperature T_L = 85 K by assuming a molecular velocity distribution function for the incident velocity $\hat{f}_{in}$, which represents a net condensation of molecules.

In regard to the condensation coefficient α_c in the non-equilibrium state, Kon et al. reported that the value of α_c slightly changed when the net condensation occurred in the vapor temperature range of approximately 85–120 K [8]. To confirm whether the same tendency as that in their study can be obtained from $\hat{\alpha}_c(\zeta_{in})$ in Fig 9b, we calculate α_c in the vapor temperatures at 85 K and 120 K with the fixed liquid temperature T_L = 85 K. The two Maxwellians at 85 K and 120 K are shown as the normalized functions of $\zeta_z\hat{f}^*(T = 85\ \mathrm{K})$ and $\zeta_z\hat{f}^*(T = 120\ \mathrm{K})$ in Fig 9b, and the incident velocities ξ_{in} in both functions were normalized by the most probable speed of the Maxwellian at T_L = 85 K. The Maxwellian at T_L = 120 K assumes non-equilibrium condensation where the incident molecules enter the liquid phase with the velocity distribution function $\zeta_z\hat{f}^*(T = 120\ \mathrm{K})$. As the liquid temperature was set at T_L = 85 K in this study, the calculation of α_c from Eq 15 with the molecular velocity distribution function $\zeta_z\hat{f}^*(T = 85\ \mathrm{K})$ yields α_c = 0.864 as shown before. This value means the condensation coefficient in the equilibrium state. In the case of the non-equilibrium state where the molecular velocity distribution function in Eq 15 was $\zeta_z\hat{f}^*(T = 120\ \mathrm{K})$, α_c was calculated as 0.878. The value of α_c obtained from Eq 15 varied slightly as expected when the system was non-equilibrium, and a slight increase in the value of α_c in the non-equilibrium system was reported in the previous study [8]. However, there is no significant difference between the calculated values of α_c in each system state. Therefore, although the condensation coefficient depends on the incident velocity of molecules as shown in Fig 9b, we conclude that the value of the condensation coefficient is almost constant regardless of whether the system is equilibrium or non-equilibrium.

We investigated the condensation coefficient α_c in terms of the incident velocity of molecules with the mass flux of colliding molecules J_{coll} in this study. By defining the mass flux of outgoing molecules J^*_{out} within the outgoing velocity range of $A < \xi_z < B$ in the same way as the J^{A-B}_{coll} in Eq 12, the discussion in this subsection can be applied to investigate the dependence of the evaporation coefficient α_e on molecular velocities.

4 Conclusion

In this study, we conducted MD simulations to discuss the position of the liquid boundary for the classification of molecules in the vicinity of the vapor–liquid interface to construct the KBCs. Because we had set the liquid boundary at $\bar{z} \approx -1.0$ in our previous studies, we investigated the validity of this position based on the molecular variables t_{stay} and z_{reach}, which characterize their motions in the vapor–liquid interface. To obtain the criterion for classifying molecules depending on these two variables, we used the *k*-means method of data clustering in which molecules were classified into clusters according to the similarity of the two variables. The results of the *k*-means method and the bivariate histogram that represents the relationship between the t_{stay} and z_{reach} of molecules show that we do not necessarily have to include t_{stay} in the classification criteria. Moreover, by considering the distribution of the t_{stay} of molecules whose z_{reach} values were in the vicinity of the vapor–liquid interface, we confirmed that most of the molecules with short t_{stay} values were classified as the reflection molecules when the liquid boundary was set at $\bar{z} \approx -1.0$. Therefore, we concluded that the liquid boundary at

$\bar{z} \approx -1.0$ applied in our previous studies yields a reasonable classification of molecules for the construction of KBCs.

Furthermore, we also investigated the relationship between the condensability of molecules and their incident velocities at the liquid phase. We found that molecules with a low incident velocity were reflected in the vicinity of the vapor boundary, and molecule whose incident velocity was near the mean velocity of the Maxwellian basically reached the liquid phase and condensed into it. Because it indicates the dependence of the condensation of molecules on their incident velocity, we calculated the condensation coefficient as a function of the incident velocity: $\hat{\alpha}_c(\zeta_{in})$. As a result, the value of $\hat{\alpha}_c(\zeta_{in})$ became small in the low-incident-velocity range, and it showed a constant value when the incident velocity exceeded the most probable speed of the Maxwellian. We also calculated α_c in the non-equilibrium system where the net condensation occurred, and we confirmed that α_c had almost the same value as that in the equilibrium system.

Supporting information

S1 Appendix. The *k*-means method.
(PDF)

Author Contributions

Conceptualization: Hirofumi Tabe, Kazumichi Kobayashi.

Data curation: Hirofumi Tabe.

Formal analysis: Hirofumi Tabe.

Funding acquisition: Kazumichi Kobayashi.

Investigation: Hirofumi Tabe.

Methodology: Hirofumi Tabe, Kazumichi Kobayashi.

Project administration: Kazumichi Kobayashi.

Resources: Kazumichi Kobayashi.

Software: Hirofumi Tabe, Kazumichi Kobayashi.

Supervision: Kazumichi Kobayashi, Hiroyuki Fujii, Masao Watanabe.

Validation: Hirofumi Tabe, Kazumichi Kobayashi.

Visualization: Hirofumi Tabe.

Writing – original draft: Hirofumi Tabe.

Writing – review & editing: Hirofumi Tabe, Kazumichi Kobayashi, Hiroyuki Fujii, Masao Watanabe.

References

1. Bird GA, Brady J. Molecular gas dynamics and the direct simulation of gas flows. vol. 5. Clarendon press Oxford; 1994.
2. Cercignani C. Rarefied gas dynamics: from basic concepts to actual calculations. vol. 21. Cambridge University Press; 2000.
3. Sone Y. Molecular gas dynamics: theory, techniques, and applications. Springer Science & Business Media; 2007.

4. Kobayashi K, Nagayama T, Watanabe M, Fujii H, Kon M. Molecular gas dynamics analysis on condensation coefficient of vapour during gas–vapour bubble collapse. Journal of Fluid Mechanics. 2018; 856:1045–1063. https://doi.org/10.1017/jfm.2018.722
5. Yamamoto K, Kobayashi K, Watanabe M, Fujii H, Kon M, Takahira H. Influence of a small amount of noncondensable gas on shock wave generation inside a collapsing vapor bubble. Physical Review Fluids. 2019; 4(6):063603. https://doi.org/10.1103/PhysRevFluids.4.063603
6. Levashov VY, Kryukov AP, Shishkova IN. Influence of the noncondensable component on the characteristics of temperature change and the intensity of water droplet evaporation. International Journal of Heat and Mass Transfer. 2018; 127:115–122. https://doi.org/10.1016/j.ijheatmasstransfer.2018.07.069
7. Lu Z, Kinefuchi I, Wilke KL, Vaartstra G, Wang EN. A unified relationship for evaporation kinetics at low Mach numbers. Nature communications. 2019; 10(1):1–8. https://doi.org/10.1038/s41467-019-10209-w PMID: 31147534
8. Kon M, Kobayashi K, Watanabe M. Method of determining kinetic boundary conditions in net evaporation/condensation. Physics of Fluids. 2014; 26(7):072003. https://doi.org/10.1063/1.4890523
9. Ishiyama T, Yano T, Fujikawa S. Molecular dynamics study of kinetic boundary condition at an interface between argon vapor and its condensed phase. Physics of Fluids. 2004; 16(8):2899–2906. https://doi.org/10.1063/1.1763936
10. Ishiyama T, Yano T, Fujikawa S. Kinetic boundary condition at a vapor-liquid interface. Physical review letters. 2005; 95(8):084504. https://doi.org/10.1103/PhysRevLett.95.084504 PMID: 16196864
11. Kon M, Kobayashi K, Watanabe M. Liquid temperature dependence of kinetic boundary condition at vapor–liquid interface. International Journal of Heat and Mass Transfer. 2016; 99:317–326. https://doi.org/10.1016/j.ijheatmasstransfer.2016.03.088
12. Kobayashi K, Hori K, Kon M, Sasaki K, Watanabe M. Molecular dynamics study on evaporation and reflection of monatomic molecules to construct kinetic boundary condition in vapor–liquid equilibria. Heat and Mass Transfer. 2016; 52(9):1851–1859. https://doi.org/10.1007/s00231-015-1700-6
13. Kobayashi K, Sasaki K, Kon M, Fujii H, Watanabe M. Kinetic boundary conditions for vapor–gas binary mixture. Microfluidics and Nanofluidics. 2017; 21(3):53. https://doi.org/10.1007/s10404-017-1887-6
14. Ishiyama T, Yano T, Fujikawa S. Molecular dynamics study of kinetic boundary condition at an interface between a polyatomic vapor and its condensed phase. Physics of Fluids. 2004; 16(12):4713–4726. https://doi.org/10.1063/1.1811674
15. Meland R, Frezzotti A, Ytrehus T, Hafskjold B. Nonequilibrium molecular-dynamics simulation of net evaporation and net condensation, and evaluation of the gas-kinetic boundary condition at the interphase. Physics of Fluids. 2004; 16(2):223–243. https://doi.org/10.1063/1.1630797
16. Yang T, Pan C. Molecular dynamics simulation of a thin water layer evaporation and evaporation coefficient. International journal of heat and mass transfer. 2005; 48(17):3516–3526. https://doi.org/10.1016/j.ijheatmasstransfer.2005.03.015
17. Louden P, Schoenborn R, Lawrence C. Molecular dynamics simulations of the condensation coefficient of water. Fluid phase equilibria. 2013; 349:83–86. https://doi.org/10.1016/j.fluid.2013.04.006
18. Nagata Y, Usui K, Bonn M. Molecular mechanism of water evaporation. Physical review letters. 2015; 115(23):236102. https://doi.org/10.1103/PhysRevLett.115.236102 PMID: 26684127
19. Kryukov A, Levashov VY. Boundary conditions on the vapor liquid interface at strong condensation. Heat and Mass Transfer. 2016; 52(7):1393–1401. https://doi.org/10.1007/s00231-015-1658-4
20. Zhakhovsky VV, Kryukov AP, Levashov VY, Shishkova IN, Anisimov SI. Mass and heat transfer between evaporation and condensation surfaces: Atomistic simulation and solution of Boltzmann kinetic equation. Proceedings of the national academy of sciences. 2019; 116(37):18209–18217. https://doi.org/10.1073/pnas.1714503115 PMID: 29666235
21. Frezzotti A, Gibelli L, Lorenzani S. Mean field kinetic theory description of evaporation of a fluid into vacuum. Physics of Fluids. 2005; 17(1):012102. https://doi.org/10.1063/1.1824111
22. Kon M, Kobayashi K, Watanabe M. Kinetic boundary condition in vapor–liquid two-phase system during unsteady net evaporation/condensation. European Journal of Mechanics-B/Fluids. 2017; 64:81–92. https://doi.org/10.1016/j.euromechflu.2016.12.001
23. Frezzotti A, Gibelli L, Lockerby D, Sprittles J. Mean-field kinetic theory approach to evaporation of a binary liquid into vacuum. Physical Review Fluids. 2018; 3(5):054001. https://doi.org/10.1103/PhysRevFluids.3.054001
24. Ohashi K, Kobayashi K, Fujii H, Watanabe M. Evaporation coefficient and condensation coefficient of vapor under high gas pressure conditions. Scientific Reports. 2020; 10(1):1–10. https://doi.org/10.1038/s41598-020-64905-5

25. Busuioc S, Gibelli L, Lockerby DA, Sprittles JE. Velocity distribution function of spontaneously evaporating atoms. Physical Review Fluids. 2020; 5(10):103401. https://doi.org/10.1103/PhysRevFluids.5.103401

26. Gu K, Watkins CB, Koplik J. Molecular dynamics simulation of the equilibrium liquid–vapor interphase with solidification. Fluid phase equilibria. 2010; 297(1):77–89. https://doi.org/10.1016/j.fluid.2010.06.014

27. Fujikawa S, Yano T, Watanabe M. Vapor-liquid interfaces, bubbles and droplets: fundamentals and applications. Springer Science & Business Media; 2011.

28. Allen MP, Tildesley DJ. Computer simulation of liquids. Oxford university press; 1987.

29. Lekner J, Henderson J. Theoretical determination of the thickness of a liquid-vapour interface. Physica A: Statistical Mechanics and its Applications. 1978; 94(3-4):545–558. https://doi.org/10.1016/0378-4371(78)90086-9

30. Tsuruta T, Tanaka H, Masuoka T. Condensation/evaporation coefficient and velocity distributions at liquid–vapor interface. International Journal of Heat and Mass Transfer. 1999; 42(22):4107–4116. https://doi.org/10.1016/S0017-9310(99)00081-2

31. Ball GH, Hall DJ. ISODATA, a novel method of data analysis and pattern classification. Stanford research inst Menlo Park CA; 1965.

32. MacQueen J, et al. Some methods for classification and analysis of multivariate observations. In: Proceedings of the fifth Berkeley symposium on mathematical statistics and probability. vol. 1. Oakland, CA, USA; 1967. p. 281–297.

33. Lloyd S. Least squares quantization in PCM. IEEE transactions on information theory. 1982; 28(2):129–137. https://doi.org/10.1109/TIT.1982.1056489

34. Jain AK. Data clustering: 50 years beyond K-means. Pattern recognition letters. 2010; 31(8):651–666. https://doi.org/10.1016/j.patrec.2009.09.011

35. Tsuruta T, Nagayama G. Molecular dynamics studies on the condensation coefficient of water. The Journal of Physical Chemistry B. 2004; 108(5):1736–1743. https://doi.org/10.1021/jp035885q

36. Tokunaga A, Tsuruta T. Nonequilibrium molecular dynamics study on energy accommodation coefficient on condensing liquid surface?Molecular boundary conditions for heat and mass transfer. Physics of Fluids. 2020; 32(11):112011. https://doi.org/10.1063/5.0027945